Small scale structure of homogeneous turbulent shear flow

D. Livescu[a)]
University of California, Los Alamos National Laboratory, CCS-2 MS B296, Los Alamos, New Mexico 87545

C. K. Madnia[b)]
Department of Mechanical and Aerospace Engineering, State University of New York at Buffalo, Buffalo, New York 14260

(Received 4 September 2003; accepted 15 April 2004; published online 22 June 2004)

The structure of homogeneous turbulent shear flow is studied using data generated by direct numerical simulations (DNS) and a linear analysis for both compressible and incompressible cases. At large values of the mean shear rate, the rapid distortion theory (RDT) limit is approached. Analytical solutions are found for the inviscid compressible RDT equations at long times. The RDT equations are also solved numerically for both inviscid and viscous cases. The RDT solutions, confirmed by the DNS results, show that the even order transverse derivative moments of the dilatational and solenoidal velocity fields are anisotropic, with the dilatational motions more anisotropic than their solenoidal counterparts. The results obtained for the incompressible case are similar to those obtained for the solenoidal motions in the compressible case. The DNS results also indicate an increase in the anisotropy of the even order transverse derivative moments with the order of the moment, in agreement with the RDT predictions. Although the anisotropy decreases with Reynolds number, it is likely that for higher even order moments it will persist at large values of the Reynolds number, in contrast with the postulate of local isotropy. The RDT solutions also predict that the normalized odd order transverse derivative moments of the solenoidal velocity for the compressible case and of the velocity for the incompressible case should approach a constant different than zero at large times. This prediction is supported by the DNS data. For higher odd order normalized moments, the RDT analysis suggests that the anisotropy may persist at large values of the Reynolds number, in agreement with the existent experimental data. The amplification of the dilatational kinetic energy in the direction of the mean shear and the anisotropy of the dilatational dissipation tensor found in the DNS results are also consistent with the RDT analysis. [DOI: 10.1063/1.1760771]

I. INTRODUCTION

Most turbulent flows are anisotropic at large scales. Homogeneous shear flow represents one of the simplest anisotropic flows and its study can reveal important aspects of the structure and production of the turbulent fluctuations. The high Reynolds number experiment of Shen and Warhaft[1] indicates that the higher odd order moments of the velocity derivatives may not be consistent with the postulate of local isotropy, which requires that the normalized odd order transverse derivative moments approach zero at large Reynolds numbers. This finding has important consequences, since this postulate has been central for turbulence theories and models.[2] Although direct numerical simulations (DNS) at high Reynolds numbers are not feasible yet, persistent anisotropy in the skewness of velocity derivatives has been observed earlier in the numerical results of Pumir,[3] also confirmed by Schumacher.[4]

The assumption of local isotropy also requires relations between the even order transverse derivative moments, which should satisfy $\langle(\partial u_1/\partial x_2)^{2n}\rangle = \langle(\partial u_1/\partial x_3)^{2n}\rangle$, and similar relations for u_2 and u_3. There is experimental evidence that the second order transverse derivative moments are not isotropic, especially when the mean rate of strain is significant.[5,6] Nevertheless, the anisotropy of the higher even order transverse moments of the velocity derivatives has not been examined. In this study we point out a lack of isotropy of the even order transverse derivative moments in homogeneous shear flow for both incompressible and compressible cases with increased anisotropy for higher order moments. We also show that the small scale dilatational motions are more anisotropic than their solenoidal counterparts, so that the anisotropy increases for the compressible case. Moreover, the anisotropy of the even order transverse derivative moments found in the DNS results is predicted by the rapid distortion theory (RDT) solutions. As the Reynolds number increases, the anisotropy among the transverse derivative moments is expected to decrease. Since it is shown that the anisotropy increases with the order of the moment, some anisotropy may persist for higher order moments at large values of the Reynolds number. In addition, it is shown that the linear analysis predicts that the normalized odd order transverse derivative moments of u_1 should approach a constant different than zero at large times, in agreement with the

a)Electronic mail: livescu@lanl.gov
b)Electronic mail: madnia@eng.buffalo.edu

DNS data. The RDT results suggest a persistent anisotropy of the higher odd order normalized transverse derivative moments at large Reynolds number, in agreement with the experimental findings.[1]

There are numerous experimental investigations of incompressible homogeneous shear flow,[1,7–9] however, no such study exists for the compressible case. Compressibility effects in turbulent flows are important in many practical applications ranging from combustion processes, to high speed aerodynamics, and to astrophysical phenomena. Although compressible turbulence has been the subject of intense research in the last 50 years, much less is known in comparison with incompressible turbulence.[10] In order to isolate the volume changes of the fluid elements, the velocity field is usually decomposed into a solenoidal (divergence free) part and a dilatational part. For homogeneous flows this decomposition is unique up to an additive constant, which can be taken to be zero without the loss of generality. Such decomposition in spectral space has been exploited by rapid distortion theories in studies of shock–turbulence interaction and homogeneous turbulence subject to bulk compression or uniform mean shear.[11]

For the RDT equations of incompressible homogeneous shear flow, analytical solutions in wave-number space are known for the velocity field in both viscous and inviscid cases.[12] The integration of these solutions over the wave-number space can yield predictions for various quantities in real space. In general, only for very early and long times the integrals can be evaluated analytically. Long time solutions for the velocity variances and shear stress are obtained by Moffatt[13] and Rogers.[14] The early time evolution of the flow is correctly captured by the RDT equations since the nonnormal amplification mechanism is linear in time.[15,16] However, due to the neglecting of the nonlinear terms and thus the energy cascade to small scales, the RDT predictions can become eventually very different than those of the full nonlinear equations. Nevertheless, for the incompressible case, the RDT equations correctly capture the behavior of various correlations coefficients in the fully developed flow field.[14]

For the case of compressible homogeneous shear flow in the RDT limit no analytical solutions are known. Simone *et al.*[17] performed RDT simulations of homogeneous shear flow and showed that the role of the distortion Mach number, M_d, on the time variation of the turbulent kinetic energy is consistent with that found in the DNS results. They also identified different time regimes in which the various contributions to the terms in the RDT equations in spectral space change qualitatively, which might be the reason for the difference in the early and long time influence of M_d on the kinetic energy growth. However, in the absence of analytical solutions, it is difficult to predict how each wave number will affect the result of the integration over the wave-number space. For example, for the incompressible case, Rogers[14] shows that at long times most of the contribution to the velocity variances and shear stress comes from a very narrow region in wave-number space, which shrinks in time.

The DNS results for compressible homogeneous shear flow of Blaisdell *et al.*[18] and Livescu *et al.*[19] reveal that the explicit dilatational effects tend to occur predominantly in the direction of the shear. Livescu and Madnia[20] examined the anisotropies of the solenoidal and dilatational motions for different values of the Reynolds and turbulent Mach numbers and found higher levels of anisotropy for the normal components of the dilatational dissipation tensor compared with those of the normal components of the solenoidal dissipation tensor. By examining the energy transfer leading to the anisotropy of the dilatational motions, Livescu *et al.*[19] showed that the nonlinear terms in the transport equation for the kinetic energy components do not have a significant contribution. This suggests that a linear mechanism might be responsible for the amplification of the dilatational motions in the direction of the shear.

The present study thus aims: (i) to point out a lack of isotropy of the even order transverse derivative moments for both compressible and incompressible cases and show that this anisotropy is due to a linear mechanism, (ii) to examine the ability of the linearized equations to predict the persistent anisotropy of the normalized odd order transverse derivative moments found in the experimental data, and (iii) to clarify if the amplification of the dilatational kinetic energy and dilatational dissipation in the direction of the shear are also due to a linear mechanism. Moreover, the different levels of anisotropy of the small scale dilatational and solenoidal motions for the compressible case is also discussed. Additionally, analytical solutions are presented for the RDT equations of compressible homogeneous turbulent shear flow.

The paper is organized as follows. Section II describes the governing equations and their linearization in the RDT limit. The numerical methodology for solving the full nonlinear and the RDT equations with the parameters for the cases considered is presented in Sec. III. Section IV contains an analysis of the RDT equations for compressible homogeneous shear flow. The inviscid RDT equations are solved analytically in the incompressible limit ($M_{t_0}S \to 0$) and pressure-released limit ($M_{t_0}S \to \infty$). For finite values of $M_{t_0}S$ and large times, analytical solutions are presented for the Fourier modes of pressure and velocity components. In Sec. V the analytical and numerical solutions of the RDT equations are compared with the DNS results. It is shown that the amplification of the dilatational kinetic energy in the direction of the shear and the anisotropy of the normal components of the dilatational dissipation tensor are captured by the RDT equations. Also in this section, the anisotropy of the even and odd order transverse derivative moments of the solenoidal and dilatational velocity fields for the compressible case and of the velocity field for the incompressible case are studied using DNS results and shown to be predicted by the RDT analysis. Summary and conclusions are given in Sec. VI.

II. GOVERNING EQUATIONS

The conservation equations which provide the mathematical model of the problem are the continuity, Navier–Stokes, and energy transport equations. For a compressible homogeneous shear flow (for which the mean, Favre averaged, velocity is given by $\tilde{u}_1 = Sx_2$ with S constant, $\tilde{u}_2 = 0$,

and $\tilde{u}_3=0$) after Rogallo's transformation of coordinates[21] $x_i'=B_{ij}x_j$, these equations, in their nondimensional form, become[19,22]

$$\rho_{,t}+(\rho u_j'')_{,k}B_{kj}=0, \tag{1}$$

$$(\rho u_i'')_{,t}=-\rho u_2'' S\delta_{i1}-(\rho u_i'' u_j'')_{,k}B_{kj}-p_{,k}B_{ki}+\left[\left(\tau_{ij}'+\frac{\mu}{\mathrm{Re}_0}(S\delta_{i1}\delta_{j2}+S\delta_{i2}\delta_{j1})\right)\right]_{,k}B_{kj}, \tag{2}$$

$$(\rho\phi)_{,t}=S(\tau_{12}'-\rho u_1'' u_2'')-(\rho u_j''\phi)_{,k}B_{kj}-(pu_j'')_{,k}B_{kj}+(\tau_{ij}'u_i'')_{,k}B_{kj}+\frac{1}{(\gamma-1)M_0^2\,\mathrm{Re}_0\,\mathrm{Pr}}(\mu T_{,l}B_{lj})_{,k}B_{kj}. \tag{3}$$

The stress tensor is $\tau_{ij}'=(2\mu/\mathrm{Re}_0)(s_{ij}'-\frac{1}{3}\Delta'\delta_{ij})$, where $s_{ij}'=\frac{1}{2}(u_{i,k}''B_{kj}+u_{j,k}''B_{ki})$ is the strain rate tensor, and $\Delta'=u_{i,k}''B_{ki}$ is the dilatation of the velocity fluctuations. The primary transport variables are the density ρ, velocity fluctuations (with respect to Favre average) in the x_i direction u_i'', and modified total energy $\phi\equiv[p/\rho(\gamma-1)]+\frac{1}{2}u_i''u_i''$, where p is the instantaneous pressure and the ratio of the specific heats $\gamma=1.4$. The coordinate transformation matrix has constant diagonal components $B_{ii}=\beta_i$ and the only off-diagonal nonzero component is $B_{12}=-\beta_1\,\mathrm{St}$.

The thermodynamic variables are related through the equation of state, $p=\rho T/\gamma M_0^2$, and the nondimensional viscosity is modeled by assuming a power law $\mu=T^n$, with $n=0.7$. The reference scales used to nondimensionalize the governing equations are the initial rms velocity fluctuations ($u_0=\sqrt{u_{i0}''u_{i0}''}$), initial mean temperature (T_0), initial mean density (ρ_0), and a reference length scale (l_0). Consequently, the nondimensional parameters in Eqs. (1)–(3) are the computational Reynolds number, $\mathrm{Re}_0=\rho_0u_0l_0/\mu_0$, the Prandtl number, $\mathrm{Pr}=\mu_0c_p/\kappa_0$, and the reference Mach number, $M_0=u_0/\sqrt{\gamma RT_0}$, where R is the gas constant and c_p is the specific heat at constant pressure. The reference viscosity, μ_0, and thermal diffusivity, κ_0, are assumed to be proportional to T_0^n.

For the incompressible case, the energy equation is eliminated, the continuity equation is replaced by the incompressibility constraint, and the molecular viscosity is constant. The governing equations become

$$u_{j,k}'B_{kj}=0, \tag{4}$$

$$u_{i,t}'=-u_2'S\delta_{i1}-(u_i'u_j')_{,k}B_{kj}-p_{,k}B_{ki}+\tau_{ij,k}'B_{kj}, \tag{5}$$

where u_i' are the velocity fluctuations and $\tau_{ij}'=1/\mathrm{Re}_0(u_{i,k}'B_{kj}+u_{j,k}'B_{ki})$.

The linearized nondimensional transport equations for density, ρ', velocity, u_i'', and pressure, p', fluctuations in a compressible homogeneous turbulent flow are derived by Kovasznay.[23] For the case of a homogeneous turbulent shear flow these equations correspond to the RDT limit, which assumes large values for the mean shear rate S. In the moving coordinate system defined above, the linearized equations become

$$\rho_{,t}'=-\langle\rho\rangle\Delta', \tag{6}$$

$$u_{i,t}''=-\frac{1}{\langle\rho\rangle}p_{,k}'B_{ki}-Su_2''\delta_{i1}+\frac{2\langle\mu\rangle}{\langle\rho\rangle\mathrm{Re}_0}\left(s_{ij}'-\frac{1}{3}\Delta'\delta_{ij}\right)_{,k}B_{kj}, \tag{7}$$

$$p_{,t}'=-\gamma\langle p\rangle\Delta'+\frac{4\langle\mu\rangle(\gamma-1)}{\mathrm{Re}_0}Ss_{12}'+\frac{\langle\mu\rangle}{M_0^2\,\mathrm{Re}_0\,\mathrm{Pr}}\langle T\rangle\times\left(\frac{p_{,jj}'}{\langle p\rangle}-\frac{\rho_{,jj}'}{\langle\rho\rangle}\right). \tag{8}$$

While the average density is constant in time for homogeneous shear flow, the linearized equation for the mean pressure is

$$\langle p\rangle_{,t}=\frac{\langle\mu\rangle(\gamma-1)}{\mathrm{Re}_0}S^2, \tag{9}$$

with the right-hand side of the equation given by the viscous dissipation of the mean flow.

Although in general the linearized equations form a coupled system of equations, for the inviscid case they can be decoupled (note that in this case the mean pressure becomes constant). Thus, an equation for the dilatation can be obtained by taking the divergence of Eq. (7),

$$\Delta_{,t}'=-\frac{1}{\langle\rho\rangle}p_{,jk}'B_{ji}B_{ki}-2Su_{2,k}''B_{k1}. \tag{10}$$

This equation is used to eliminate the dilatation from Eq. (8). Finally, after eliminating u_2'' with the use of Eq. (7), an equation for the pressure fluctuations is obtained,

$$\frac{p_{,ttt}'}{c_0^2}=p_{,tjk}'B_{ji}B_{ki}-4Sp_{,jk}'B_{j1}B_{k2}, \tag{11}$$

where c_0 is the initial value of the mean speed of sound $c=(\langle\gamma p\rangle/\langle\rho\rangle)^{1/2}$ (which for the inviscid case becomes constant). Equation (11) is a third order linear differential equation in time, with variable coefficients. For $S=0$ (decaying isotropic turbulence) Eq. (11) leads to a wave-like equation, with bounded solutions. For $S\neq0$, the time t can be nondimensionalized by $1/S$, so that $\eta\equiv\mathrm{St}$. Furthermore, after applying the Fourier transform, Eq. (11) yields

$$\hat{p}_{,\eta\eta\eta}=-\frac{c_0^2}{S^2}(k^2\hat{p}_{,\eta}-4k_1k_2\hat{p}), \tag{12}$$

where the wave number k_j is related to the wave number $\hat{k}_i$ in the moving coordinate system by $k_j=B_{ij}\hat{k}_i$ and $k^2=k_jk_j$. The notations used in the present paper for the wave numbers in the fixed and moving coordinate systems are the opposite of the notations used by Rogers.[14] Due to the time variation of k_2, Eq. (12) does not have an easily derived analytical solution except in the case $k_1=0$ and for very early and long times ($\eta\approx0$ and $\eta\to\infty$). Nevertheless, it should be noted that, although for the full nonlinear equations the initial turbulent Mach number, $M_{t_0}=(2K_0)^{1/2}/c_0$,

and S are independent parameters, they appear together in Eq. (12), since $c_0^2/S^2=2K_0/\langle\rho\rangle/(M_{t_0}S)^2=1/(M_{t_0}S)^2$ (note that the initial value of the turbulent kinetic energy is $K_0=0.5$ and $\langle\rho\rangle=1$). Moreover, if the distortion Mach number,[17] $M_d=SL/c$, is introduced, then $c_0^2/S^2=L_0^2/M_{d_0}^2$, where M_{d_0} is the initial value of the distortion Mach number and L_0 is the initial value of the integral scale $L=(2K)^{3/2}/\epsilon$. Similar equations, depending on c_0^2/S^2, η, the wave number, and initial conditions can be found for the Fourier modes of dilatation, density fluctuations, and velocity components. In order to complete the analysis, the initial conditions for Eq. (12) are considered. These relations can be rearranged to isolate the parameter $(M_{t_0}S)$ by making the transformation $\hat{p}'=M_{t_0}\hat{p}$,

$$\hat{p}'|_{\eta=0}=M_{t_0}\hat{p}_0, \tag{13}$$

$$\hat{p}'_{,\eta}|_{\eta=0}=-\frac{2K_0}{\langle\rho\rangle M_{t_0}S}\hat{d}_0, \tag{14}$$

$$\hat{p}'_{,\eta\eta}|_{\eta=0}=\left(-\frac{k'^2}{(M_{t_0}S)^2}(M_{t_0}\hat{p}_0)+\frac{2k_1'}{M_{t_0}S}\mathbf{i}\hat{u}_{2_0}\right)\frac{2K_0}{\langle\rho\rangle}, \tag{15}$$

where k_i' is the initial value of the wave number in the fixed coordinate system ($k_i'=\hat{k}_i$), $k'^2=k_i'k_i'$, $\mathbf{i}=\sqrt{-1}$, and $\hat{d}_0$ and $\hat{u}_{2_0}$ are the initial values of the Fourier modes of the dilatation and velocity fluctuations in the x_2 direction, respectively. It can be seen that, if the initial value of the pressure mode scales with $1/M_{t_0}$ for constant $(M_{t_0}S)$, then $\hat{p}'$ depends on $(M_{t_0}S)$ and η only. This condition is fulfilled if the pressure fluctuations are initialized with zero or from a Poisson equation, which is the case with most DNS studies of homogeneous turbulent shear flow. Note that to first order the Poisson equation becomes

$$M_{t_0}\hat{p}=2\mathbf{i}\langle\rho\rangle(M_{t_0}S)\frac{k_1}{k^2}\hat{u}_2. \tag{16}$$

In this case, from the inviscid momentum equations and Eq. (10) for the dilatation it yields, after replacing t with η, that $\hat{u}_i$ and $\hat{\Delta}$ depend only on $(M_{t_0}S)$. Moreover, if the initial values of the density fluctuations are set to zero, $S\hat{\rho}$ will also be a function of $(M_{t_0}S)$, wave number, and η only.

As a result, for the initializations usually used in the DNS of homogeneous turbulent shear flow, the inviscid linearized theory predicts the existence of only one compressibility parameter $(M_{t_0}S)$, for the properly scaled variables. However, the addition of either the nonlinear or the viscous terms prevents the governing equations to be written in terms of only one compressibility parameter. Therefore, for moderate values of S or Reynolds number, two independent compressibility parameters can be defined. Nevertheless, as pointed out by Simone *et al.*,[17] changes in M_{d_0} at constant M_{t_0} are more important to the growth of turbulent kinetic energy than changes in M_{t_0} at constant M_{d_0}.

TABLE I. Parameters for the DNS cases.

Case	Re_{λ_0}	S_0^*	M_{d_0}[a]
1	21	4.86	1.46
2	21	7.29	2.19
3	21	9.71	2.91
4	21	14.6	4.37
5	21	21.9	6.56
6	50	17.4	5.22

[a]Values corresponding to the compressible cases. All compressible cases have $M_{t_0}=0.3$.

III. NUMERICAL SOLUTION PROCEDURE

A. DNS methodology

Equations (1)–(3) are solved using the Fourier pseudospectral method with Rogallo's remeshing technique.[21] Details can be found in Livescu *et al.*[19] All simulations are performed within a box containing 256^3 points. The computational domain is twice as long in the streamwise direction as in the cross-stream and spanwise directions so that $\beta_1=0.5$, $\beta_2=1.0$, and $\beta_3=1.0$. The initial velocity is a random solenoidal field with unity rms and the spectrum given by $E(k)=k^4/k_{0v}^5\exp(-2k^2/k_{0v}^2)$ with $k_{0v}=10$. The initial pressure fluctuations are evaluated from a Poisson equation, the initial density field is uniform, and the initial value of the mean pressure is calculated from the mean equation of state. The numerical method, mesh size, and initial conditions for pressure and velocity fields are the same for the incompressible case.

Several cases, 1–5, are considered at different values of the mean shear rate. For each case two simulations, one compressible and one incompressible, are performed. Table I presents the relevant information for each of the cases considered. The initial nondimensional shear rate is defined as $S_0^*=2KS/\epsilon$. For the compressible cases, the distortion Mach number M_{d_0} is also listed. Cases 1–5 have the initial value of the Taylor Reynolds number $\mathrm{Re}_{\lambda_0}=21$ and it increases to $\mathrm{Re}_\lambda\sim100$ at the end of the simulations. Additionally, one more case (case 6) is considered with $\mathrm{Re}_{\lambda_0}=50$, and all the other parameters as those of case 2. In the next sections, the compressible simulations corresponding to cases 1–6 are labeled C1–C6, and the incompressible cases are labeled I1–I6. All simulations were monitored to ensure that the integral scales remain small compared to the box size and the Kolmogorov microscale is larger than the grid size. The compressible runs were also repeated with initial turbulent Mach numbers ranging from $M_{t_0}=0.1$ to $M_{t_0}=0.6$ and all the results presented in the next sections remained qualitatively unchanged.

Based on the magnitude of the shear rate, a simple scaling argument can be used to characterize the relative importance of the nonlinear term in the momentum equations compared to the linear term arising from the presence of the nonzero mean velocity gradient. Thus, as shown in Ref. 24, the nonlinear term is negligible when $S_1^*/\mathrm{Re}_{\lambda_1}\gg1/8$ and dominates when $S_1^*/\mathrm{Re}_{\lambda_1}\ll0.35$, where $S_1^*=u'^2S/\epsilon$ and $\mathrm{Re}_{\lambda_1}=u'^2/(\nu\sqrt{\langle u_{1,1}^2\rangle})$, with $u'=\sqrt{\langle u_1^2\rangle}$. Figure 1 shows the

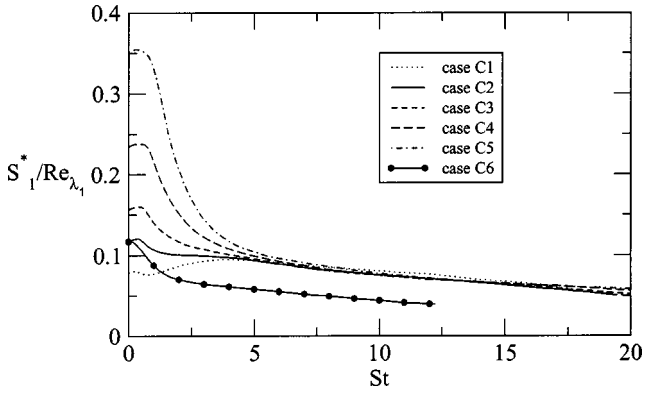

FIG. 1. Time evolution of $S_1^*/\mathrm{Re}_{\lambda_1}$.

time evolution of $S_1^*/\mathrm{Re}_{\lambda_1}$ for the compressible cases considered. The results obtained for the incompressible cases are close. The initial range of variation covers the region in which both the linear and nonlinear terms in the momentum equations are important, with case C1, with lowest shear, for which the nonlinear effects dominate and case C5, with highest shear, for which the linear term becomes more important. After a development time the results obtained for the cases with different values of the mean shear rate become close, while retaining the dependence on the initial Reynolds number. For all cases, the late time values of $S_1^*/\mathrm{Re}_{\lambda_1}$ are in the region where the nonlinear effects dominate, based on the scaling arguments given in Ref. 24.

B. RDT methodology

The unknowns in Eqs. (6)–(8) are transformed into[17]

$$\hat{f}_1(\mathbf{k},\eta)=\frac{k_1\hat{u}_3-k_3\hat{u}_1}{m}, \tag{17}$$

$$\hat{f}_2(\mathbf{k},\eta)=(k_1\hat{u}_1+k_3\hat{u}_3)\frac{k_2}{mk}-\frac{m}{k}\hat{u}_2, \tag{18}$$

$$\hat{f}_3(\mathbf{k},\eta)=\frac{k_1\hat{u}_1+k_2\hat{u}_2+k_3\hat{u}_3}{k}=\frac{\hat{\Delta}}{\mathbf{i}k}, \tag{19}$$

$$\hat{f}_4(\mathbf{k},\eta)=\mathbf{i}\hat{p}, \tag{20}$$

$$\hat{f}_5(\mathbf{k},\eta)=\mathbf{i}\hat{\rho}, \tag{21}$$

where $m=\sqrt{k_1^2+k_3^2}$. $\hat{f}_1$ is the component of the velocity along the perpendicular on the plane defined by the wave-number vector and the k_2 direction. $\hat{f}_2$ is the component along the k_2 direction so that $\hat{f}_1$ and $\hat{f}_2$ form the solenoidal velocity and $\hat{f}_3$ is the projection of the velocity on the wave-number vector and corresponds to the dilatational part of the velocity. Additionally, since the equations are linear, a matrix exponentiation method can be used by letting $\hat{f}_i(\mathbf{k},\eta)=g_{ij}(\mathbf{k},\eta)\hat{f}_j(\mathbf{k},0)$, with $g_{ij}(\mathbf{k},0)=\delta_{ij}$.

The resulting system for the unknowns g_{ij} becomes

$$g_{1j,\eta}=-\frac{k_3}{k}g_{2j}+\frac{k_2k_3}{mk}g_{3j}-\frac{\langle\mu\rangle}{\mathrm{Re}_0\langle\rho\rangle S}k^2g_{1j}, \tag{22}$$

$$g_{2j,\eta}=\frac{k_1k_2}{k^2}g_{2j}-\frac{k_1}{m}g_{3j}-\frac{\langle\mu\rangle}{\mathrm{Re}_0\langle\rho\rangle S}k^2g_{2j}, \tag{23}$$

$$g_{3j,\eta}=2\frac{k_1m}{k^2}g_{2j}-\frac{k_1k_2}{kk^2}g_{3j}-\frac{k}{\langle\rho\rangle S}-\frac{4}{3}\frac{\langle\mu\rangle}{\mathrm{Re}_0\langle\rho\rangle S}k^2g_{3j}, \tag{24}$$

$$g_{4j,\eta}=\frac{\gamma\langle p\rangle}{S}kg_{3j}+\frac{2\langle\mu\rangle}{\mathrm{Re}_0}(\gamma-1)\left(-\frac{k_1k_3}{m}g_{1j}+\frac{k_1k_2^2}{km}g_{2j}+2\frac{k_1k_3}{k}g_{3j}\right)-\frac{\langle\mu\rangle}{M_{t_0}^2\,\mathrm{Re}_0\,\mathrm{Pr}\,S}k^2\left(\frac{g_{4j}}{\langle p\rangle}-\frac{g_{5j}}{\langle\rho\rangle}\right), \tag{25}$$

$$g_{5j,\eta}=\frac{\langle\rho\rangle}{S}kg_{3j}, \tag{26}$$

where $j=\overline{1,5}$. The system (22)–(26) is transformed into spherical coordinates by setting $k_1'=k'\cos\alpha$, $k_2'=k'\sin\alpha\sin\phi$, and $k_3'=k'\sin\alpha\cos\phi$. Cases with $(101\times602\times204)$ grid points for the coordinates (k',α,ϕ) are considered. The discretization is nonuniform, allowing for more grid points near the line $\alpha=\phi=\pi/2$. This is necessary, as explained in the next section, in order to correctly capture a local peak of some of the unknowns, which gives an important contribution to their integral over the wave-number space. A fourth-order Runge–Kutta scheme is employed for the time advancement. The equations are also solved for the incompressible case (which is recovered by letting $\hat{f}_3=0$). It should be noted that the system (22)–(26) is independent of the initial spectra, so that it is solved only once for a particu-

TABLE II. Initial conditions for the linearized equations.

Type of initial conditions	$\hat{p}\|_{\eta=0}$	χ_0
L1	Poisson equation	0
L2	0	0
L3	Poisson equation	0.1
L4	Acoustic equilibrium	0.1

lar set of parameters. Furthermore, when integrating over the wave-number space only the initial power spectra are required, and not the phase information.

The linearized Eqs. (22)–(26) are solved for different values of S_0^* ranging from 7.24 to 362. For all compressible cases $M_{t_0}=0.3$, so that the range in S_0^* corresponds to $2.2<M_{d_0}<109$. This range extends from a low shear case in which the nonlinear effects in the corresponding DNS case are important to cases with very high shear. The initial velocity power spectrum is the same as in the DNS simulations described earlier. For the compressible case, for each value of $(M_{t_0}S)$ four types of initial conditions, labeled L1–L4, are considered (Table II). For cases L1 and L3 the pressure fluctuations are initialized from a Poisson equation, while for cases with L2 initial conditions they are set to zero. The initial velocity field is solenoidal for cases L1 and L2 while $\chi_0=K_{d0}/K_0=0.1$ for cases L3 and L4, where K_{d0} is the initial dilatational kinetic energy. For cases with L4 initial conditions the strong form of the acoustic equilibrium is considered,[17] so that there is an equipartition of energy between the potential and kinetic energies of the dilatational component at each wave number. Therefore the initial pressure power spectrum is given by $E_p(k')=\sqrt{\gamma\langle p\rangle|_{t=0}\langle\rho_0\rangle}E_d(k')$, where E_d is the initial power spectrum of the dilatational velocity. For each case, both the inviscid and viscous equations are solved. The types of initial conditions considered are not exhaustive for the initial conditions used in DNS of compressible turbulence (e.g., see Refs. 25 and 26 for decaying isotropic turbulence). However, they were chosen such that the role of a nonzero initial dilatational field can be isolated. In the next sections, the numerical solutions of the RDT equations are compared with the DNS results and with the analytical predictions.

IV. ANALYTICAL RESULTS

By examining Eq. (12) for the pressure mode three cases can be identified based on the values of $1/(M_{t_0}S)^2$.

A. "Pressure-released" limit $[1/(M_{t_0}S)^2\to 0]$

This case corresponds to values of the distortion Mach number approaching infinity. After integrating Eq. (12), a quadratic dependence on η is obtained. However, when the initial conditions (13)–(15) simplified for large $(M_{t_0}S)$ are applied, the solution is obtained as $\hat{p}=\hat{p}|_{\eta=0}$. Since the pressure mode is multiplied by the factor $1/(M_{t_0}S)$ in the transport equations for the velocity modes, it can be dropped from these equations. Therefore the equations for the velocity modes become

$$\hat{u}_{1,\eta}=-\hat{u}_2,\quad \hat{u}_{2,\eta}=0,\quad \hat{u}_{3,\eta}=0 \tag{27}$$

with the solutions $\hat{u}_1=\hat{u}_2|_{\eta=0}\eta+\hat{u}_1|_{\eta=0}$, $\hat{u}_2=\hat{u}_2|_{\eta=0}$, and $\hat{u}_3=\hat{u}_3|_{\eta=0}$. After integrating over the wave-number space, it is obtained that the kinetic energy in x_1 direction increases quadratically, while it remains constant in the other two directions. This case corresponds to the "pressure-released" limit discussed by Cambon *et al.*[27] and Simone *et al.*[17]

B. Incompressible case $[1/(M_{t_0}S)^2\to\infty]$

Since S is assumed large in the RDT limit, as $1/(M_{t_0}S)^2\to\infty$ it yields $M_{t_0}\to 0$, so that the incompressible case is recovered. The transport equation for the pressure mode becomes

$$k^2\hat{p}_{,\eta}-4k_1k_2\hat{p}=0. \tag{28}$$

The solution is straightforward and can be written as

$$\hat{p}=\hat{p}|_{\eta=0}\frac{k'^4}{k^4}, \tag{29}$$

with $\hat{p}|_{\eta=0}=2\mathbf{i}S(k_1'/k'^2)\hat{u}_2|_{\eta=0}$. In order to find the pressure variance from Eq. (29), the integration over the wave-number space should be performed numerically. Analytical expressions can be obtained to approximate the time behavior of the pressure variance only for $\eta\to 0$ (early time) and $\eta\to\infty$ (long time). In both cases the integration is conveniently done in spherical coordinates. The procedure is similar to that used by Townsend[12] and Rogers[14] to find the time dependence of velocity and scalar one point statistics in incompressible turbulent shear flow. After the transformation $k_1'=k'\cos\alpha$, $k_2'=k'\sin\alpha\sin\phi$, $k_3'=k'\sin\alpha\cos\phi$, and $d\mathbf{k}'=k'^2\sin\alpha\,d\alpha\,d\phi\,dk'$, for isotropic initial conditions [so that $|\hat{u}_2|_{\eta=0}|^2=[E(k')/4\pi k'^2][(k_1'^2+k_3'^2)/k'^2]$ with $E(k')$ the initial velocity power spectrum], the pressure spectrum function becomes

$$\mathbf{\Phi_p}(\mathbf{k}')=\frac{E(k')}{4\pi k'^2}\times\frac{4S^2\cos^2\alpha(\cos^2\alpha+\sin^2\alpha\cos^2\phi)}{k'^2(1-2\eta\cos\alpha\sin\alpha\sin\phi+\eta^2\cos^2\alpha)^4}, \tag{30}$$

and the pressure variance can be found from

$$\langle p'^2\rangle(\eta)=\frac{(2\pi)^3}{V}\int_{-\infty}^{\infty}\mathbf{\Phi_p}\,dk_i'. \tag{31}$$

For small values of η (early time) the integrand can be expanded in a Taylor series in η, which can be integrated analytically. It yields

$$\frac{\langle p'^2\rangle}{q}=\frac{4}{15}+\frac{8}{105}\eta^2+\cdots, \tag{32}$$

where $q=4S^2\int[E(k')/k'^2]dk'$. In terms of the initial value of the pressure variance the dependence is $\langle p'^2\rangle/\langle p_0'^2\rangle=1+\frac{2}{7}\eta^2+\cdots$.

As explained by Rogers,[14] the long time behavior cannot be obtained using the same procedure, since expanding around $\eta=\infty$ yields a result which is not uniformly valid over the entire domain. This can be easily seen by evaluating $\hat{p}$ for $k_2'=1$, $k_3'=0$, and $k_1'=1/\eta$, which for $\eta\to\infty$ yields

$$\lim_{\eta\to\infty}\hat{p}(k_1'=1/\eta,\eta)=\infty. \tag{33}$$

Therefore a significant contribution to the integral of the pressure spectrum over the wave number space comes from a narrow region near $k_1'=0$ which decreases in size as η increases. Following Rogers,[14] the asymptotic behavior can be found by dividing the domain into two regions, an inner region located around $\eta k_1'=O(1)$ (which corresponds to $\alpha=\pi/2$) and an outer region consisting of the rest of the domain covered by $0\leqslant\alpha\leqslant\pi$ and $0\leqslant\phi\leqslant2\pi$. In the inner region, around $\alpha=\pi/2$ and $\phi=\pi/2$, $\mathbf{\Phi_p}(\mathbf{k}')k'^2\sin\alpha$ has a peak. The magnitude of the peak and the extent in α and ϕ over which it occurs can be found by writing $\alpha=\pi/2-\epsilon_\alpha$ and $\phi=\pi/2-\epsilon_\phi$ and expanding the sin and cos functions in the expression for the pressure spectrum. It yields that $\mathbf{\Phi_p}(\mathbf{k}')k'^2\sin\alpha$ is of order η^4 for $\epsilon_\alpha=1/\eta\pm O(1/\eta^2)$ and $\epsilon_\phi=O(1/\eta)$, so that the peak occurs over a region of extent $O(1/\eta^2)$ in α and $O(1/\eta)$ in ϕ. This indicates a linear increase for the pressure variance. The correct behavior can be obtained by combining the results from the inner and outer regions. The result obtained remains $\langle p'^2\rangle/\langle p_0'^2\rangle\sim\eta$, also supported by the results of the numerical integration.

C. $1/(M_{t_0}S)^2$ finite

In this case the transport equation for the pressure mode [Eq. (12)] remains third order, and does not have an easily derived analytical solution. However, some limiting cases can be found. First, it should be observed that $\hat{p}$ approaches zero as $k_i'\to\infty$ so that only finite values of k_i' are of interest. Then for small values of η the equation reduces to an equation with constant coefficients which can be easily solved. However, since the roots of the characteristic polynomial are dependent on the parameter $(M_{t_0}S)$, the analytical computations involving the integration of the solution over the wave-number space are cumbersome. Nevertheless, the solution was verified numerically and it agrees reasonably well with the full numerical solution of the RDT equations.

As $\eta\to\infty$, unlike in the incompressible case, the behavior of the Fourier modes in the outer region ($k_1'\eta\gg1$) is very important for the integration over the wave-number space. It is shown above that for the incompressible case the contribution from the inner region yields a linear increase for the pressure variance. However, as the parameter $1/(M_{t_0}S)^2$ decreases, the peak of the pressure mode occurring in the inner region decreases its magnitude (Fig. 2) and the contribution from this region to the pressure variance yields a less than linear increase in time. This contribution to the pressure variance is negligible at long times since it is shown below that the contribution from the outer region leads to a linear increase in the pressure variance.

In the outer region $k_1'\eta\to\infty$ for $\eta\to\infty$ and Eq. (12) becomes

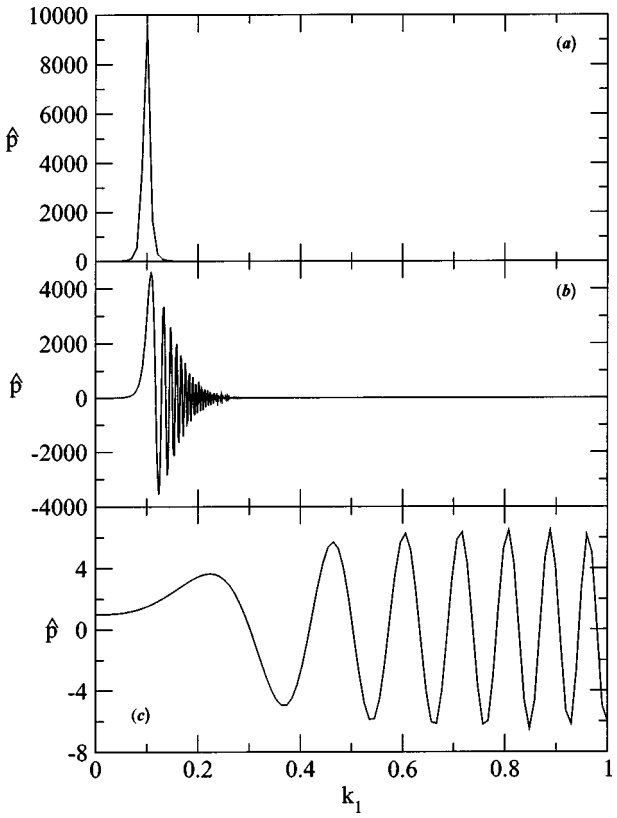

FIG. 2. Compressibility effects on the k_1' variation of the pressure mode. Inviscid case, $\eta=10$, $k_2=1$, $k_3=0$, with initial conditions $\hat{p}|_{\eta=0}=1$, $\hat{p}_{,\eta}|_{\eta=0}=0$, and $\hat{p}_{,\eta\eta}|_{\eta=0}=0$. (a) Incompressible, (b) compressible, $M_{t_0}S=0.01$, and (c) compressible, $M_{t_0}S=1$.

$$\hat{p}_{,\eta\eta\eta}=-\frac{2K_0k_1'^2}{\langle\rho\rangle(M_{t_0}S)^2}(\eta^2\hat{p}_{,\eta}+4\eta\hat{p}). \tag{34}$$

The solution of Eq. (34) can be written as $\hat{p}=\phi_1\hat{p}|_{\eta=0}+\phi_2\hat{p}_{,\eta}|_{\eta=0}+\phi_3\hat{p}_{,\eta\eta}|_{\eta=0}$, with ϕ_i given by the formulas

$$\phi_1={}_1F_2\left([1],\left[\frac{1}{2},\frac{3}{4}\right],-\frac{1}{4}\zeta^2\right), \tag{35}$$

$$\phi_2=J_{-1/4}(\zeta)(\zeta/2)^{3/4}2\Gamma\left(\frac{3}{4}\right)\left(\frac{M_{t_0}S}{k_1'}\right)^{1/2}\left(\frac{\langle\rho\rangle}{2K_0}\right)^{1/4}, \tag{36}$$

$$\phi_3=J_{1/4}(\zeta)(\zeta/2)^{3/4}\Gamma\left(\frac{1}{4}\right)\frac{M_{t_0}S}{2k_1'}\left(\frac{\langle\rho\rangle}{2K_0}\right)^{1/2}, \tag{37}$$

where ${}_1F_2$ and J_ν represent a generalized hypergeometric function and the Bessel function of the first kind of order ν, respectively, Γ is the gamma function and $\zeta=(k_1'\eta^2/M_{t_0}S)\sqrt{K_0/2\langle\rho\rangle}$. For large values of the nondimensional time η, using the asymptotic expansions for these functions given in Ref. 28, it is obtained that

$$\phi_1\approx-(\zeta/2)^{1/4}\sin\left(\zeta-\frac{3\pi}{8}\right)\Gamma\left(\frac{3}{4}\right), \tag{38}$$

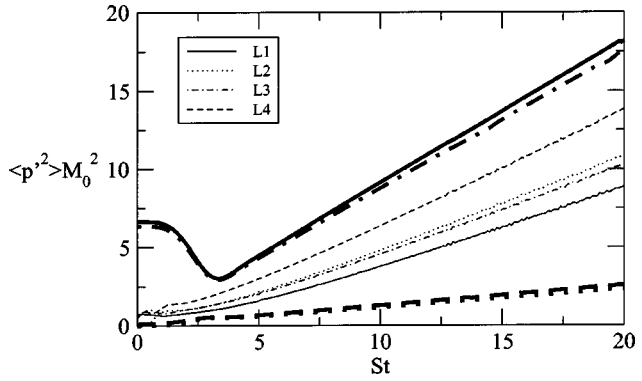

FIG. 3. Numerical solution of the inviscid RDT equations for the pressure variance for $M_{t_0}S=4.6$ (thin lines) and $M_{t_0}S=31$ (thick lines) and different initial conditions. For clarity the results obtained for $M_{t_0}S=4.6$ are magnified 5 times.

$$\phi_2 \approx (\zeta/2)^{1/4}\cos\left(\zeta-\frac{\pi}{8}\right)2\Gamma\left(\frac{3}{4}\right)\left(\frac{M_{t_0}S}{\pi k_1'}\right)^{1/2}\left(\frac{\langle\rho\rangle}{2K_0}\right)^{1/4}, \tag{39}$$

$$\phi_3 \approx (\zeta/2)^{1/4}\cos\left(\zeta-\frac{3\pi}{8}\right)\Gamma\left(\frac{1}{4}\right)\frac{M_{t_0}S}{2\sqrt{\pi}k_1'}\left(\frac{\langle\rho\rangle}{2K_0}\right)^{1/2}. \tag{40}$$

These expressions indicate that the Fourier mode of the pressure oscillates in time and the amplitude of the oscillations increases as $\sqrt{\eta}$. In order to find the pressure variance, the integration over the wave-number space can be performed using the Riemann–Lebesgue theorem, $\int_a^b f(k')e^{\mathbf{i}k'\eta}dk' \to 0$ as $\eta\to\infty$ provided that $\int_a^b|f(k')|dk'$ exists. Since $\sin^2\alpha=(1-\cos 2\alpha)/2$ and $\cos^2\alpha=(1+\cos 2\alpha)/2$, the integration yields a linear increase in time for the pressure variance. This is consistent with the numerical solutions of the linearized inviscid equations presented in Fig. 3.

Similar to the pressure variance, it can be shown that for finite values of $1/(M_{t_0}S)^2$, most of the contribution to the dilatation variance and kinetic energy in x_2 direction, K_2, comes from the outer region. From the solution obtained for the pressure mode, approximations for the asymptotic behavior of the dilatation and u_2 velocity modes in the outer region can be derived using the following equations:

$$\hat{\Delta}=-\frac{(M_{t_0}S)}{2K_0}\hat{p}'_{,\eta}, \tag{41}$$

$$\hat{u}_2=\frac{\mathbf{i}\hat{\Delta}_{,\eta}}{2k_1}-\frac{\mathbf{i}k^2\hat{p}'}{2\langle\rho\rangle(M_{t_0}S)k_1}. \tag{42}$$

The relations obtained are $\hat{\Delta}=\phi_{1\Delta}\hat{p}'|_{\eta=0}+\phi_{2\Delta}\hat{p}'_{,\eta}|_{\eta=0}+\phi_{3\Delta}\hat{p}'_{,\eta\eta}|_{\eta=0}$ and $\hat{u}_2=\phi_{1u2}\hat{p}'|_{\eta=0}+\phi_{2u2}\hat{p}'_{,\eta}|_{\eta=0}+\phi_{3u2}\hat{p}'_{,\eta\eta}|_{\eta=0}$ with $\phi_{i\Delta}$ and ϕ_{iu2} given by

$$\phi_{1\Delta} \approx (\zeta/2)^{3/4}\cos\left(\zeta-\frac{3\pi}{8}\right)\Gamma\left(\frac{3}{4}\right)\left(\frac{k_1'^2M_{t_0}^2S^2}{2\langle\rho\rangle K_0^3}\right)^{1/4}, \tag{43}$$

$$\phi_{2\Delta} \approx (\zeta/2)^{3/4}\sin\left(\zeta-\frac{\pi}{8}\right)\Gamma\left(\frac{3}{4}\right)\frac{M_{t_0}S}{\sqrt{2\pi}K_0}, \tag{44}$$

$$\phi_{3\Delta} \approx (\zeta/2)^{3/4}\sin\left(\zeta-\frac{3\pi}{8}\right)\Gamma\left(\frac{1}{4}\right)\frac{1}{4}\left(\frac{M_{t_0}^3S^3}{\pi k_1'}\right)^{1/2}\times\left(\frac{\langle\rho\rangle}{8K_0^5}\right)^{1/4}, \tag{45}$$

$$\phi_{1u2} \approx \mathbf{i}(\zeta/2)^{1/4}\cos\left(\zeta-\frac{3\pi}{8}\right)\Gamma\left(\frac{3}{4}\right)\frac{k_1'}{2\langle\rho\rangle M_{t_0}S}, \tag{46}$$

$$\phi_{2u2} \approx \mathbf{i}(\zeta/2)^{1/4}\sin\left(\zeta-\frac{\pi}{8}\right)\Gamma\left(\frac{3}{4}\right)\left(\frac{k_1'}{\pi M_{t_0}S}\right)^{1/2}\frac{1}{2K_0}, \tag{47}$$

$$\phi_{3u2} \approx \mathbf{i}(\zeta/2)^{1/4}\sin\left(\zeta-\frac{3\pi}{8}\right)\Gamma\left(\frac{1}{4}\right)\frac{1}{4}\left(\frac{1}{2\pi\langle\rho\rangle K_0}\right)^{1/2}. \tag{48}$$

Again, using the Riemann–Lebesgue theorem, Eqs. (43)–(48) can be integrated over the wave-number space to yield an η^3 increase in time for the dilatation variance, $\langle\Delta'^2\rangle$, and a linear increase for $\langle u_2^2\rangle$. This represents an important difference compared to the incompressible case, where it is known that for large times the u_2 velocity variance decreases in time as $\ln(4\eta)/(4\eta)$.[14] It is shown below that the increase in time in the compressible case is due to the dilatational component.

In the incompressible case, the influence from the inner region to $\langle u_1^2\rangle$ and $\langle u_3^2\rangle$ is significant and at large times $\langle u_1^2\rangle \approx 2\ln 2\eta$ and $\langle u_3^2\rangle \approx \pi^2/8\ln\eta - C$.[14] For the compressible case, after using the approximation $k_2 \approx -\eta k_1'$, the transport equations for $\hat{u}_1$ and $\hat{u}_3$ can be solved analytically and for large values of η,

$$\hat{u}_1 \sim \hat{u}_1|_{\eta=0}+\frac{d_1}{\sqrt{\eta}}\sin\left(\frac{k_1'\eta^2}{M_{t_0}S}\sqrt{\frac{K_0}{2\langle\rho\rangle}}+d_2\right), \tag{49}$$

$$\hat{u}_3 \sim \hat{u}_3|_{\eta=0}+\frac{e_1}{\sqrt{\eta}}\sin\left(\frac{k_1'\eta^2}{M_{t_0}S}\sqrt{\frac{K_0}{2\langle\rho\rangle}}+e_2\right), \tag{50}$$

with the coefficients d_i and e_i depending on $(M_{t_0}S)$ and the wave number. Therefore, in the outer region, for large times, $\hat{u}_1$ and $\hat{u}_3$ become constant. Numerical solutions of the RDT equations indicate that the contributions from the inner region to $\langle u_1^2\rangle$ and $\langle u_3^2\rangle$ remain dominant for the compressible case and K_1 and K_3 increase in time, as shown in Fig. 4. However, as the compressibility parameter $M_{t_0}S$ increases, these contributions decrease their importance resulting in a reduced rate of increase of the turbulent kinetic energy in x_1 and x_3 directions. This explains the ''stabilizing'' effect of compressibility on the evolution of the turbulent kinetic energy found in the RDT study of Simone *et al.*[17]

From the solution corresponding to the Fourier mode of the dilatation, the dilatational parts of the velocity modes can be obtained as $\hat{u}_{i_d}=-\mathbf{i}k_i/k^2\hat{\Delta}$. Numerical solutions of the RDT equations indicate that the inner region has a negligible contribution to the variances of the dilatational velocity components. In the outer region, for large values of η, the time variation of the dilatational parts of the velocity modes can be derived from formulas (43)–(45) as

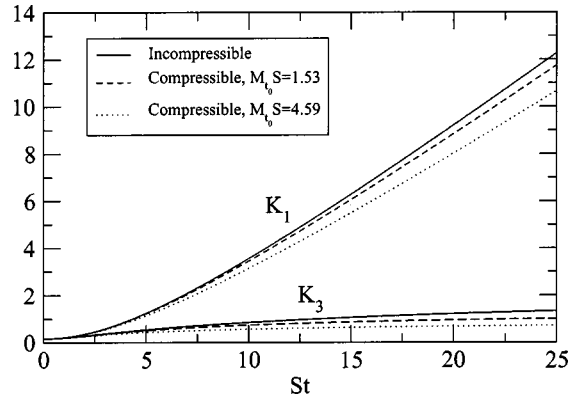

FIG. 4. Compressibility effect on the kinetic energy in x_1 and x_3 directions. Inviscid case, with L1 initial conditions.

$$\hat{u}_{1_d} \sim \frac{c_{11}}{\sqrt{\eta}} \sin\left(\frac{k_1' \eta^2}{M_{t_0} S} \sqrt{\frac{K_0}{2\langle \rho \rangle}} + c_{12} \right), \tag{51}$$

$$\hat{u}_{2_d} \sim c_{21} \sqrt{\eta} \sin\left(\frac{k_1' \eta^2}{M_{t_0} S} \sqrt{\frac{K_0}{2\langle \rho \rangle}} + c_{22} \right), \tag{52}$$

$$\hat{u}_{3_d} \sim \frac{c_{31}}{\sqrt{\eta}} \sin\left(\frac{k_1' \eta^2}{M_{t_0} S} \sqrt{\frac{K_0}{2\langle \rho \rangle}} + c_{23} \right), \tag{53}$$

where the constants c_{ij} depend on $(M_{t_0}S)$ and the wave number.

V. COMPARISON WITH DNS

Although the early time response of the flow to the presence of the shear is correctly captured by the linearized equations, the long time evolution of the flow can become very different than that obtained from the full nonlinear equations. However, there are quantities which follow the RDT predictions even at long times. This is the case with various correlation coefficients (e.g., the Reynolds stress correlation coefficient) in the incompressible case.[14] For the compressible case, the effect of compressibility on the evolution of the turbulent kinetic energy is correctly captured by the linearized equations.[17]

It is shown below that other characteristics of the dilatational field are captured by the linearized equations. In particular, it is shown that the amplification of the dilatational kinetic energy in the direction of the shear and the anisotropy of the normal components of the dilatational dissipation rate tensor are captured by the RDT equations. Furthermore, DNS results show that the transverse even order derivative moments of the velocity field in both compressible and incompressible cases are anisotropic and the anisotropy increases with the order of the moment. Thus, the anisotropy of the higher order moments may persist at large values of the Reynolds number, in contrast with the local isotropy principle.[29] Moreover, the DNS results indicate that the odd order normalized x_2 derivative moments of u_1 approach a constant different than zero at large times. These results can also be explained using the RDT solutions.

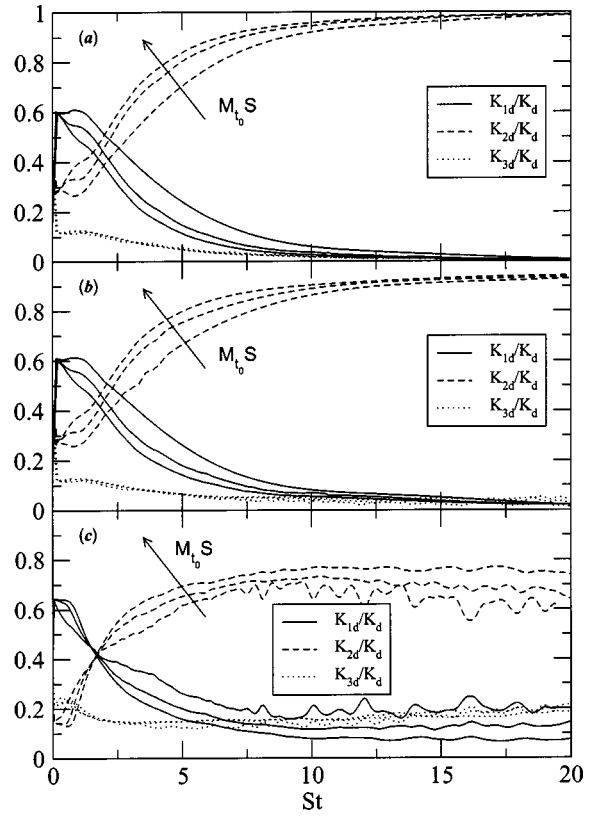

FIG. 5. Time evolution of the normalized dilatational kinetic energy components for $M_{t_0}S=1.53$, 3.1, and 4.6. (a) Inviscid RDT, (b) viscous RDT, and (c) DNS. The curves correspond to cases C2, C4, and C5.

A. Dilatational kinetic energy and dissipation anisotropy

By comparing formulas (51)–(53) with solutions obtained for the velocity modes, it can be seen that at long times $\hat{u}_1 \approx \hat{u}_{1_s}$, $\hat{u}_2 \approx \hat{u}_{2_d}$, and $\hat{u}_3 \approx \hat{u}_{3_s}$. It is obtained that most of the dilatational kinetic energy resides in the direction of the mean velocity gradient, consistent with the numerical solution of the linearized Eqs. (6)–(8) [Fig. 5(a)]. The addition of the viscous terms decreases the dominance of K_{2_d} component compared to the other two components, as can be seen in Fig. 5(b). A further decrease of the relative magnitude of K_{2_d} is obtained in the fully nonlinear case [Fig. 5(c)]. Nevertheless, as Fig. 5(c) shows, the dilatational kinetic energy in the direction of the mean velocity gradient obtained in DNS is larger than in the other two directions, in agreement with the previous studies.[18,19,30] The above analysis indicates that the amplification of the dilatational kinetic energy in the direction of the mean shear can be explained by linear effects.

Previous numerical simulations of compressible homogeneous shear flow[18–20] indicate that the dilatational dissipation rate tensor behaves very differently than its solenoidal counterpart. Thus, the dilatational dissipation rate is amplified in the direction of the mean shear. This behavior was previously attributed to the formation of shocklets aligned preferentially in x_2 direction. Livescu and Madnia[20] performed simulations at different values of the turbulent Mach

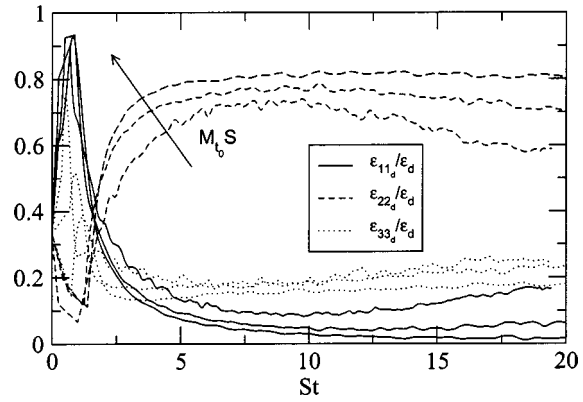

FIG. 6. Time variation of the diagonal components of the dilatational dissipation rate tensor for $M_{t_0}S=1.53$, 3.1, and 4.6, corresponding to cases C2, C4, and C5.

number and obtained no significant decrease in the anisotropy of the dilatational dissipation rate tensor in low turbulent Mach number simulations. Therefore, the amplification of the dilatational dissipation rate in the direction of the mean shear is not associated with the presence of shocklets. This conclusion is also obtained in Ref. 31. Figure 6 shows that ϵ_{22_d} becomes more important compared to ϵ_{11_d} and ϵ_{33_d} as $M_{t_0}S$, which is proportional to the distortion Mach number, increases. After multiplying the solutions for the dilatational velocity modes [Eqs. (51)–(53)] by $\mathbf{i}k_i$ and performing the integration over the wave-number space, it can be seen that in the RDT limit $\langle(\partial u_{2_d}/\partial x_2)(\partial u_{2_d}/\partial x_2)\rangle$ becomes much larger than $\langle(\partial u_{1_d}/\partial x_1)(\partial u_{1_d}/\partial x_1)\rangle$ and $\langle(\partial u_{3_d}/\partial x_3)\times(\partial u_{3_d}/\partial x_3)\rangle$. Numerical solutions of the RDT equations in both inviscid and viscous cases confirm this result. Therefore, the anisotropy of the normal components of the dilatational dissipation rate tensor can be associated with a linear mechanism.

B. Higher order derivative moments

In the outer region k_2 increases continuously, while it is very small in the inner region (where $k_1'\eta \approx k_2'$). Using the solutions provided in the preceding section for the solenoidal and dilatational components of the velocities, it can be shown that after the multiplication by k_2, the contribution from the outer region becomes dominant at long times. Therefore, the x_2 derivatives of the velocity components become much larger than the derivatives in the other two directions. As a result, all the even order derivative statistics involving x_2 derivatives become amplified and this effect is more pronounced for higher order statistics. Figure 7 compares moments of the transverse derivatives, $\langle(\partial u_{1_d}/\partial x_j)^n\rangle$ where $j=2$, 3 and $n=2$, 4, and 6, of the dilatational velocity in the x_1 direction. It can be seen that, as the distortion Mach number increases and the RDT limit is approached, the moments containing x_2 derivatives become much larger than the corresponding x_3 derivative statistics. Moreover, in agreement with the RDT predictions, this anisotropy is strongly amplified for higher order moments. This again suggests that the small scale anisotropy of the dilatational motions found

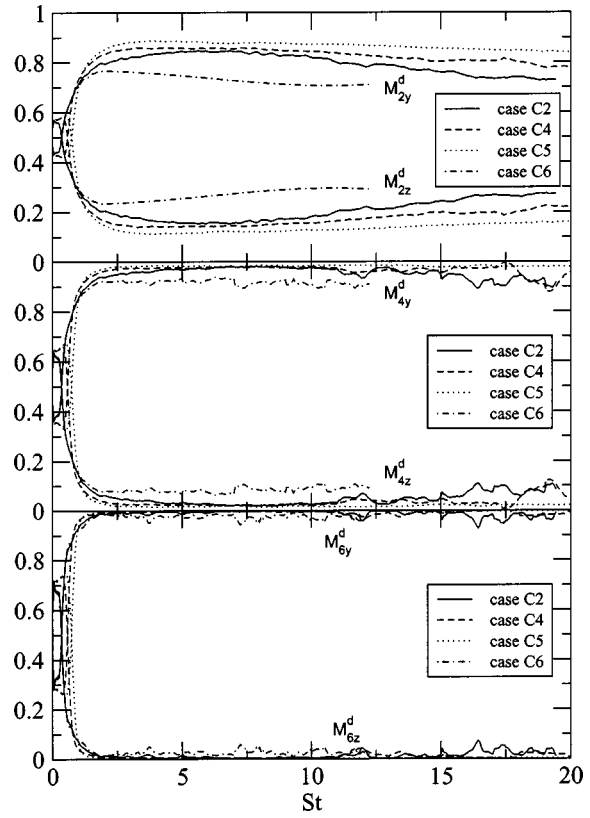

FIG. 7. Even order transverse derivative moments of the dilatational velocity in x_1 direction, $M_{ny}^d=\langle(\partial u_{1_d}/\partial x_2)^n\rangle/(\langle(\partial u_{1_d}/\partial x_2)^n\rangle+\langle(\partial u_{1_d}/\partial x_3)^n\rangle)$ and $M_{nz}^d=\langle(\partial u_{1_d}/\partial x_3)^n\rangle/(\langle(\partial u_{1_d}/\partial x_2)^n\rangle+\langle(\partial u_{1_d}/\partial x_3)^n\rangle)$. (a) $n=2$, (b) $n=4$, and (c) $n=6$.

in the DNS results is produced by a linear mechanism. On the other hand, the results presented show that the higher order transverse moments are increasingly more anisotropic as the order of the moment increases. Thus, even if the anisotropy decreases with Reynolds number, some degree of anisotropy will persist for higher order transverse derivative moments at large values of the Reynolds number.

Although the inner region has a significant contribution to the one-point statistics of the solenoidal velocity components in x_1 and x_3 directions, this contribution becomes negligible for the statistics involving x_2 derivatives. As explained above, in the outer region $\hat{u}_{1_s}$ and $\hat{u}_{3_s}$ become constant at large times so that after the multiplication with k_2 they increase linearly. Therefore, the outer region yields a quadratic increase in time for $\langle(\partial u_{1_s}/\partial x_2)(\partial u_{1_s}/\partial x_2)\rangle$ and $\langle(\partial u_{3_s}/\partial x_2)(\partial u_{3_s}/\partial x_2)\rangle$. The contribution from the inner region does not increase after the multiplication with k_2 and the inner region yields a less than quadratic increase for the above quantities. Similar results are obtained for higher order moments. Thus, similar to the dilatational velocities, in the RDT limit the even order transverse derivatives of the solenoidal velocities in x_1 and x_3 directions are anisotropic and become even more anisotropic as the order of the statistics increases. Figure 8 confirms that this effect is also present in the DNS results for the derivative moments of u_{1_s} and similar results are obtained for the derivative moments of u_{3_s}.

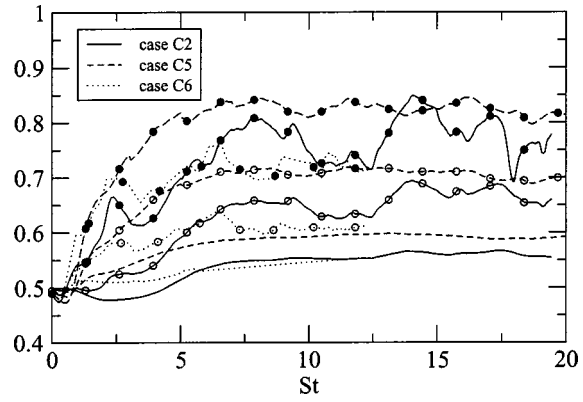

FIG. 8. Even order transverse derivative moments of the solenoidal velocity in x_1 direction, $M^s_{ny}=\langle(\partial u_{1_s}/\partial x_2)^n\rangle/(\langle(\partial u_{1_s}/\partial x_2)^n\rangle+\langle(\partial u_{1_s}/\partial x_3)^n\rangle)$. $n=2$ (no symbols), $n=4$ (open symbols), and $n=6$ (closed symbols).

A comparison between Figs. 7 and 8 indicates that the transverse solenoidal derivative moments are less anisotropic than their dilatational counterparts. Again, it can be shown that this is also in agreement with the RDT predictions. Thus, since $\hat{u}_{1_s}$ becomes constant in the outer region, it yields that $k_2\hat{u}_{1_s}\sim\eta$ and $\langle(\partial u_{1_s}/\partial x_2)^2\rangle\sim\eta^2$. However, the x_3 derivative retains influence mostly from the inner region and $\langle(\partial u_{1_s}/\partial x_3)^2\rangle\sim\eta$. On the other hand $\hat{u}_{1_d}$ retains influence mostly from the outer region. The Riemann–Lebesgue theorem can be used to integrate formula (51) multiplied by k_2 and k_3 to obtain for the dilatational component that $\langle(\partial u_{1_d}/\partial x_2)^2\rangle\sim\eta$ and $\langle(\partial u_{1_d}/\partial x_3)^2\rangle\sim 1/\eta$. Similar results are obtained for higher order statistics. Therefore, in the RDT limit, the even order transverse derivatives of the u_{1d} are more anisotropic than their solenoidal counterparts for large but finite values of η (Fig. 9). Similar results are obtained for the velocity in the x_3 direction.

Using the same analysis as above, it can be shown that the odd order moments of the x_2 derivatives of u_{1_s} also have most of the contributions from the outer regions. Thus, after the multiplication with $k_2^n\approx(-\eta k_1')^n$, the solution in the outer region becomes much larger than that obtained in the inner region as $\eta\to\infty$. Note that $|u_{1_s}|$ increases in time as $\eta^{1/2}$ in the inner region and the multiplication by k_2 does not

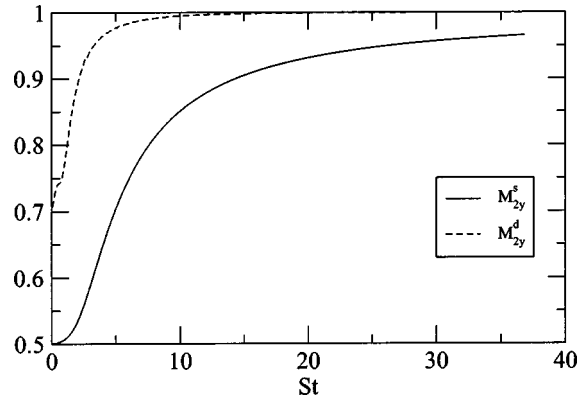

FIG. 9. RDT results for the second order transverse derivatives of u_{1_s} and u_{1_d}. L1 initial conditions, $M_{t_0}S=1.53$.

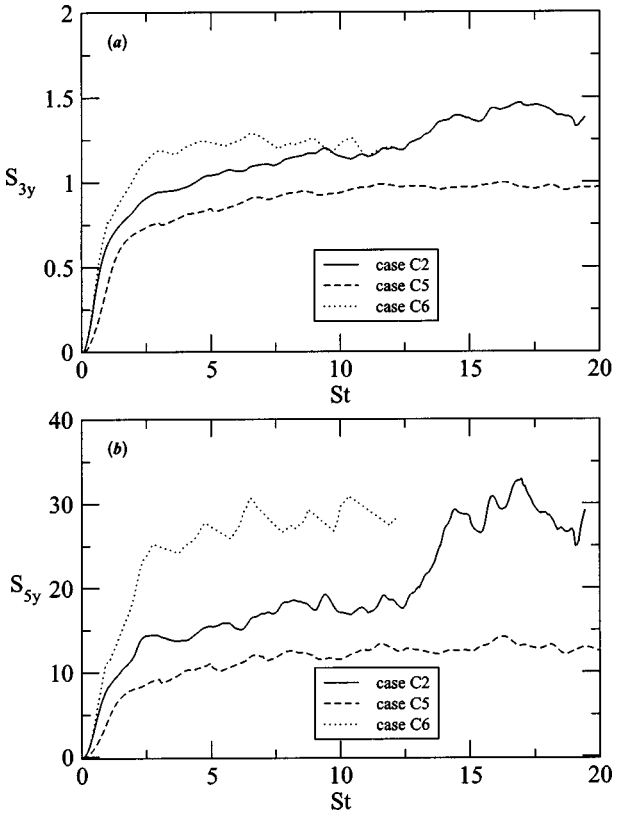

FIG. 10. Odd order normalized transverse derivative moments of the solenoidal velocity in x_1 direction, $S_{ny}=\langle(\partial u_{1_s}/\partial x_2)^n\rangle/(\langle(\partial u_{1_s}/\partial x_2)^2\rangle)^{n/2}$. (a) $n=3$, (b) $n=5$.

increase this rate. Since in the outer region $\hat{u}_{1_s}$ becomes constant at large times, it yields that the moment of order n increases in time as η^n, and, therefore, the normalized odd order moments, $\langle(\partial u_{1_s}/\partial x_2)^n\rangle/[\langle(\partial u_{1_s}/\partial x_2)^2\rangle]^{n/2}$, with n odd, should approach a constant different than zero at large times. As Fig. 10 shows, this prediction is in general agreement with the DNS data. The same analysis cannot be used for u_{3_s}. It was shown that in the outer region $\hat{u}_{3_s}$ approaches its initial value. Therefore, after multiplication by $k_2^n\approx(-\eta k_1')^n$ the odd order moments of the x_2 derivative, would approach values proportional to those of the initial odd order moments of the x_1 derivative. However, for isotropic initial conditions, these values are zero. This is consistent with the overall symmetry of the problem, which requires that the odd order x_1 and x_2 moments of the u_3 velocity remain zero at all times.

For the incompressible case, complete analytical solutions are known for the velocity field.[12,14] Although most of the contributions to the velocity variances in x_1 and x_3 directions come from the inner region, it is easy to show that the statistics involving x_2 derivatives have contributions mostly from the outer region, where at large times $k_2\approx-\eta k_1'$. Moreover, the behavior of the velocity modes in the outer region is similar to that obtained above for the solenoidal velocity modes. Consequently, in the RDT limit the transverse even order moments of the velocity derivatives are anisotropic, and the anisotropy increases for higher order moments. Similar to the solenoidal moments for the

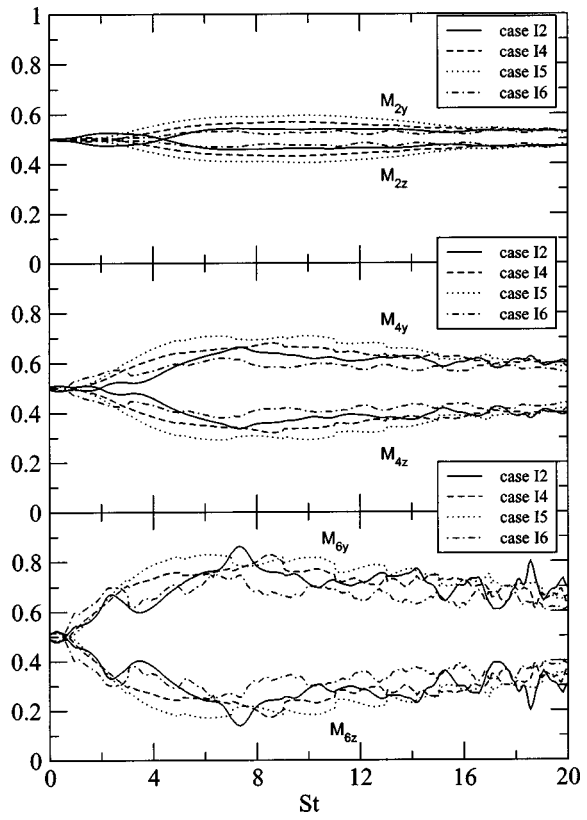

FIG. 11. Even order transverse derivative moments of the velocity in x_1 direction, incompressible case. $M_{ny}=\langle(\partial u_1/\partial x_2)^n\rangle/(\langle(\partial u_1/\partial x_2)^n\rangle+\langle(\partial u_1/\partial x_3)^n\rangle)$ and $M_{nz}=\langle(\partial u_1/\partial x_3)^n\rangle/(\langle(\partial u_1/\partial x_2)^n\rangle+\langle(\partial u_1/\partial x_3)^n\rangle)$. (a) $n=2$, (b) $n=4$, and (c) $n=6$.

compressible case and consistent with the RDT predictions, the incompressible DNS results presented in Fig. 11 show an increase in the anisotropy for higher order transverse derivatives moments of u_1. Similar results are obtained for u_3. Therefore, it is expected that for higher order moments the anisotropy will persist at large Reynolds numbers.

In addition, similar to the solenoidal velocity for the compressible case, the RDT solutions for the incompressible case predict that the odd order normalized x_2 derivative moments of u_1 and u_3 should approach a constant different than zero at large times. The DNS results are similar to those shown in Fig. 10 for the solenoidal velocity field in the compressible case and support the RDT prediction. As explained above, as the Reynolds number increases the small scales become more energetic and the flow departs from the RDT limit (see also Fig. 1). For very large values of the Reynolds number, the postulate of local isotropy requires that the odd order transverse derivative moments should approach zero. However, since the linear effects lead to a η^n increase in time for the x_2 derivative moments, for higher order moments the linear contribution may become dominant at long times even at large values of the Reynolds number. Therefore, the higher order normalized transverse x_2 derivative moments could have persistent nonzero values at large Reynolds numbers. The present numerical simulations do not have a large enough Reynolds number to examine this hypothesis, however the analysis presented is consistent with the experimental results of Shen and Warhaft.[1] At high Reynolds numbers, the experimental results indicate that lower odd order moments of $\partial u_1/\partial x_2$ become small as the Reynolds number increases. However, this tendency is not observed for higher order moments. As suggested by Schumacher *et al.*,[24] the small-scale intermittency might play a role on the observed behavior of the higher order moments. Nevertheless, the persistent anisotropy of the higher odd order normalized derivative moments found experimentally is in agreement with the present linear analysis.

VI. SUMMARY AND CONCLUSIONS

The structure of homogeneous turbulent shear flow is studied using data generated by DNS and an RDT analysis for both compressible and incompressible cases. For the compressible case, simulations with different initial values of the distortion Mach number, M_d, and Reynolds number are considered. Incompressible simulations are performed with the same initial pressure and velocity fields as for the compressible simulations.

Previous DNS studies[18–20] indicate that there is an anisotropy among the dilatational kinetic energy components. Moreover, the results of Livescu *et al.*[19] suggest that the energy transfer through the nonlinear terms in the transport equations for K_{i_d} is not responsible for this behavior. In order to verify that the anisotropy of the dilatational kinetic energy components can be explained by linear effects, the linearized equations are considered. The RDT equations are solved numerically, for both the inviscid and viscous cases, for a large range of distortion Mach numbers and different types of initial conditions. The RDT results are consistent with the DNS findings for the development of the dilatational field.

Furthermore, for large times, analytical solutions are found for the inviscid linearized equations in Fourier space. The integration of these solutions over the wave-number space can predict the behavior of various statistics in real space. It is shown that the solutions for the pressure, dilatation and dilatational velocities of the Fourier modes for finite values of k_1' oscillate in time and the amplitudes of oscillations increase. The analytical relations indicate that the magnitude of the Fourier mode of the dilatational velocity in the direction of the mean shear becomes much larger than in the other two directions.

It is known that for incompressible homogeneous turbulent shear flow in the RDT limit most of the contributions to the velocity variances come from a narrow region in the wave-number space situated near $k_1'=0$.[14] A similar trend is found for the pressure variance. However, it is shown that the contribution from this region to the statistics of the velocity field involving x_2 derivatives for both compressible and incompressible cases and to all the statistics of the dilatational velocities becomes negligible at long times. For finite values of k_1', the wave number in the direction of the mean shear increases continuously in time. Therefore, the derivatives in this direction become much larger than in the other two directions. As a result, in the RDT limit the even order transverse derivative moments of both the dilatational and solenoidal velocity fields for the compressible case and

the even order transverse derivative moments of the velocity field for the incompressible case are anisotropic. Moreover, the anisotropy becomes amplified for higher order moments. The RDT analytical solutions also predict that the small dilatational scales are more anisotropic than their solenoidal counterparts, in agreement with the DNS results. Since the x_2 derivatives of the velocity field retain influence mostly from the region where the wave number in the x_2 direction increases in time, it is shown that in the RDT limit the odd order normalized x_2 derivative moments of u_1 for the incompressible case and u_{1_s} for the compressible case should approach a constant different than zero at large times. This prediction is consistent with the DNS results.

As the Reynolds number increases the small scales become more energetic and for constant mean distortion the flow departs the RDT limit. Therefore, it is expected that, consistent with the postulate of local isotropy, the anisotropy of the small scales should decrease at large values of the Reynolds number, i.e., the odd order normalized x_2 derivative moments approach zero and the even order transverse moments become isotropic. However, it is argued that, since in the RDT limit the odd order moments increase in time as η^n, where n is the order of the moment, for higher order moments the linear contribution may be important even at large values of the Reynolds number. Thus, the RDT analysis suggests a persistent anisotropy of the higher odd order normalized derivative moments. In addition, since the anisotropy of the even order transverse derivative moments increases with the order of the moment, it is expected that persistent anisotropy levels in the transverse higher even order derivative moments will be found at large values of the Reynolds number. Although high Reynolds number results will not be available from DNS in the near future, they are within the reach of experiments and these predictions can be verified using experimental data.

ACKNOWLEDGMENTS

This work was sponsored by the Donors of the Petroleum Research Funds administrated by the American Chemical Society under Grants No. 35064-AC9 and No. 38333-AC9, and the US Department of Energy. Computational resources were provided by the National Center for Supercomputer Applications at the University of Illinois Urbana-Champaign, the Center for Computational Research at State University of New York at Buffalo, and through the Institutional Computing Project, Los Alamos National Laboratory.

[1] X. Shen and Z. Warhaft, ''The anisotropy of the small scale structure in high Reynolds number ($R_\lambda \approx 1000$) turbulent shear flow,'' Phys. Fluids **12**, 2976 (2000).
[2] K. R. Sreenivasan and R. A. Antonia, ''The phenomenology of small-scale turbulence,'' Annu. Rev. Fluid Mech. **29**, 435 (1997).
[3] A. Pumir, ''Turbulence in homogeneous shear flows,'' Phys. Fluids **8**, 3112 (1996).
[4] J. Schumacher, ''Derivative moments in stationary homogeneous shear turbulence,'' J. Fluid Mech. **441**, 109 (2001).
[5] L. W. B. Browne and R. A. Antonia, ''Turbulent energy dissipation in a wake,'' J. Fluid Mech. **179**, 307 (1987).
[6] T. Zhou, R. A. Antonia, J.-J. Lasserre, M. Coantic, and F. Anselmet, ''Transverse velocity and temperature derivative measurements in grid turbulence,'' Exp. Fluids **34**, 449 (2003).
[7] S. Garg and Z. Warhaft, ''On the small scale structure of simple shear flow,'' Phys. Fluids **10**, 662 (1998).
[8] S. Tavoularis and S. Corrsin, ''Experiments in nearly homogeneous turbulent shear flow with a uniform mean temperature gradient. Part 1,'' J. Fluid Mech. **204**, 457 (1981).
[9] S. Tavoularis and U. Karnik, ''Further experiments on the evolution of turbulent stresses and scales in uniformly sheared turbulence,'' J. Fluid Mech. **204**, 457 (1989).
[10] S. K. Lele, ''Compressibility effects on turbulence,'' Annu. Rev. Fluid Mech. **26**, 211 (1994).
[11] C. Cambon and J. F. Scott, ''Linear and nonlinear models of anisotropic turbulence,'' Annu. Rev. Fluid Mech. **31**, 1 (1999).
[12] A. A. Townsend, *The Structure of Turbulent Shear Flow*, 2nd ed. (Cambridge University Press, Cambridge, 1976).
[13] H. K. Moffatt, in *Proceedings of the International Conference on Atmospheric Turbulence and Radio Wave Propagation, Moscow, June, 1965*, edited by A. M. Yaglom and V. I. Tartarski (Nauka, Moscow, 1967), p. 139.
[14] M. M. Rogers, ''The structure of a passive scalar field with a uniform mean gradient in rapidly sheared homogeneous turbulent flow,'' Phys. Fluids A **3**, 144 (1991).
[15] J. M. Hamilton, J. Kim, and F. Waleffe, ''Regeneration mechanisms of near-wall turbulence structures,'' J. Fluid Mech. **287**, 317 (1995).
[16] F. Waleffe, ''On a self sustaining process in shear flows,'' Phys. Fluids **9**, 883 (1997).
[17] A. Simone, G. N. Coleman, and C. Cambon, ''The effect of compressibility on turbulent shear flow: a rapid-distortion-theory and direct-numerical-simulation study,'' J. Fluid Mech. **330**, 307 (1997).
[18] G. A. Blaisdell, N. N. Mansour, and W. C. Reynolds, ''Numerical simulations of compressible homogeneous turbulence,'' Report No. TF-50 (Department of Mechanical Engineering, Stanford University, Stanford, CA, 1991).
[19] D. Livescu, F. A. Jaberi, and C. K. Madnia, ''The effects of heat release on the energy exchange in reacting turbulent shear flow,'' J. Fluid Mech. **450**, 35 (2002).
[20] D. Livescu and C. K. Madnia, ''Anisotropy of turbulent reacting shear flow,'' in *DNS/LES Progress and Challenges*, edited by C. Liu, L. Sakell, and T. Beutner (Greyden, Columbus, OH, 2001).
[21] R. S. Rogallo, ''Numerical experiments in homogeneous turbulence,'' NASA Tech. Mem. 81315 (1981).
[22] G. A. Blaisdell, N. N. Mansour, and W. C. Reynolds, ''Compressibility effects on the growth and structure of homogeneous turbulent shear flows,'' J. Fluid Mech. **256**, 443 (1993).
[23] L. S. G. Kovasznay, ''Turbulence in supersonic flow,'' J. Aeronaut. Sci. **20**, 657 (1953).
[24] J. Schumacher, K. R. Sreenivasan, and P. K. Yeung, ''Derivative moments in turbulent shear flows,'' Phys. Fluids **15**, 84 (2003).
[25] J. R. Ristorcelli and G. A. Blaisdell, ''Consistent initial conditions for the DNS of compressible turbulence,'' Phys. Fluids **9**, 4 (1997).
[26] R. Samtaney, D. I. Pullin, and B. Kosovic, ''Direct numerical simulations of decaying compressible turbulence and shocklet statistics,'' Phys. Fluids **13**, 1415 (2001).
[27] C. Cambon, G. N. Coleman, and N. N. Mansour, ''Rapid distortion analysis and direct simulation of compressible homogeneous turbulence at finite Mach number,'' J. Fluid Mech. **257**, 641 (1993).
[28] I. S. Gradshteyn and I. M. Ryzhik, *Table of Integrals, Series, and Products*, 6th ed. (Academic, New York, 2000).
[29] A. S. Monin and A. M. Yaglom, *Statistical Fluid Mechanics: Mechanics of Turbulence* (MIT Press, Cambridge, 1975).
[30] R. Friedrich and F. P. Bertolotti, ''Compressibility effects due to turbulent fluctuations,'' Appl. Sci. Res. **57**, 165 (1997).
[31] G. A. Blaisdell and O. Zeman, ''Investigation of the dilatational dissipation in compressible homogeneous shear flow,'' *Proceedings of the 1992 CTR Summer Program, CTR, Stanford/NASA Ames* (Stanford University, Stanford, CA, 1992), p. 231.